GEOPHYSICS

Abyssal marine tectonics from the SWOT mission

Yao Yu[1]*, David T. Sandwell[1], Gerald Dibarboure[2]

The global ocean covers 71% of Earth's surface, yet the seafloor is poorly charted compared with land, the Moon, Mars, and Venus. Traditional ocean mapping uses ship-based soundings and nadir satellite radar altimetry—one limited in spatial coverage and the other in spatial resolution. The joint NASA–CNES (Centre National d'Etudes Spatiales) Surface Water and Ocean Topography (SWOT) mission uses phase-coherent, wide-swath radar altimetry to measure ocean surface heights at high precision. We show that 1 year of SWOT data offers more detailed information than 30 years of satellite nadir altimetry in marine gravity, enabling the detection of intricate seafloor structures at 8-kilometer spatial resolution. With the mission still ongoing, SWOT promises critical insights for bathymetric charting, tectonic plate reconstruction, underwater navigation, and deep ocean mixing.

The global seafloor remains one of the last unexplored frontiers within our inner Solar System. Only 25% of it has been directly surveyed by ships using multibeam echo sounders with ~200- to 400-m spatial resolution (*1*), revealing a myriad of small-scale (~1-km) features, including abyssal hills formed at seafloor spreading ridges, small seamounts created by off-ridge volcanism, and river-incised canyons on continental margins. Comprehensive knowledge of these features is vital for a wide range of scientific and practical applications, such as understanding the detailed tectonic and geologic history of deep oceans, analyzing ocean circulation and the generation and dissipation of tidally driven internal waves, modeling tsunami propagation and inundation, understanding sediment transport, studying marine ecosystems and biodiversity, improving undersea navigation and cable and pipeline routing, and sustainably managing marine resources (*2*). However, detailed surveys are expensive and time consuming. For example, in the search for Malaysia Airlines Flight 370 (MH370), bathymetric surveys from June 2014 to June 2016 were conducted covering about 279,000 km^2, which marked the largest area surveyed in the Southern Ocean (*3*). However, this area encompasses merely 0.077% of the global ocean. By contrast, three-quarters of the global seafloor has only been inferred using gravity measurements from profiling satellite altimeters, which are limited in spatial resolution (12- to 16-km full wavelength) (*4*). This indirect, coarse mapping leaves many small-scale features unresolved. Given the current pace of mapping, complete seafloor coverage by ships within this decade is improbable, particularly in the remote Southern Ocean.

The Surface Water and Ocean Topography (SWOT) (*5*) mission is a wide-swath radar altimetry system observing global water surface height. The mission bridges the gap in seafloor mapping between the high-resolution but limited coverage provided by multibeam sonar and the low-resolution but global coverage of standard radar altimeters collected over the past three decades. Launched in December 2022, SWOT uses state-of-the-art phase-coherent interferometry to measure two-dimensional sea surface heights (SSHs) with high precision. Using 1 year of SWOT ocean data, we derive a global gravity field approaching a spatial resolution of 8 km, which surpasses the resolution of the gravity model built from 30 years of nadir altimeter data. This gravity map allows for the characterization of global abyssal hills, the identification of thousands of small seamounts, and the mapping of submarine canyons at continental margins.

Constructing a global gravity field

We used SWOT's level 2 Ka-band radar interferometer (KaRIn) low-rate SSH data from April 2023 to July 2024 to construct a global vertical gravity gradient (VGG) (in Eötvös units) map. VGG, as the second-order gradient of gravitational potential, highlights short-wavelength *O* (10-km) signals and has reduced sensitivity to sediment density, which makes it ideal for seafloor structure identifications (*6*). VGG can

[1]Scripps Institution of Oceanography, University of California San Diego, La Jolla, CA, USA. [2]Centre National d'Etudes Spatiales, Toulouse, France.
*Corresponding author. Email: yayu@ucsd.edu

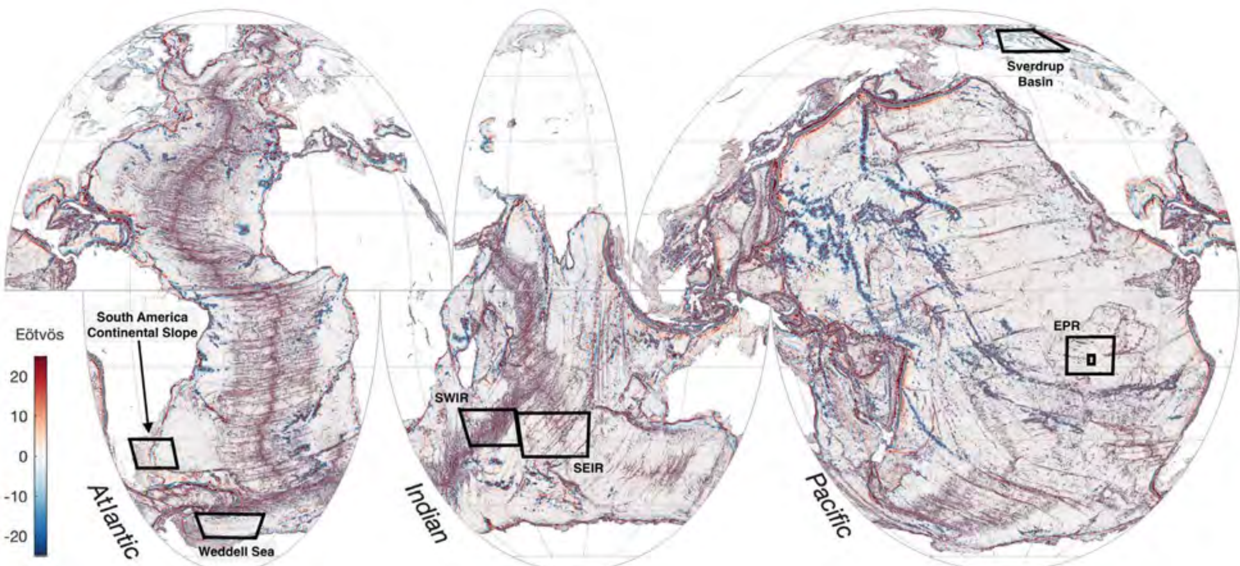

Fig. 1. Global map of SWOT VGG showing the Atlantic Ocean, the Indian Ocean, and the Pacific Ocean. Land is depicted in white. Black boxes highlight locations of the South America continental slope, Weddell Sea, SWIR, SEIR, Sverdrup Basin, and EPR, which are examined in detail in the text. 1 Eötvös = 10^{-9} s^{-2}. The full-resolution VGG model can be viewed in Google Earth and is available on Zenodo (*30*).

be calculated as the negative of the sea surface curvature, following the Laplace equation (*7*). SWOT low-rate swath data, derived from native KaRIn interferograms, underwent default low-pass Hamming filtering with a half gain at 4.5-km wavelength and was then stored on a fixed 2 km–by–2 km grid (*8*, *9*). We processed 18 cycles from the SWOT 21-day repeat science orbit and ~98 cycles from the 1-day repeat orbit to make a global VGG map (*10*), revealing seafloor features that are undetectable by traditional nadir altimeters (Fig. 1). We highlight three findings: individual abyssal hill fabrics, small seamounts with improved boundary resolution delineation, and high-resolution details of continental margin structures.

Abyssal hills

Abyssal hills (Fig. 2), which were not previously well resolved by the VGG computed from 30 years of nadir altimetry, are now individually distinguishable in SWOT data (see comparison in fig. S5). These hills, depicted as thin parallel VGG highs in red, are the most prevalent landform on Earth, formed by normal faulting along the midocean ridge axis, yet they are poorly understood (*11*, *12*). Before SWOT, abyssal hills were primarily mapped using ship sonars. With just 1 year of SWOT ocean data, individual abyssal hills are visible across most ocean basins.

At the ultraslow-spreading Southwest Indian Ridge (SWIR) (Fig. 2A), with a plate spreading rate of <20 mm/year, high-amplitude (~300-m root mean square height), wide-spaced abyssal hills are observed in multibeam sonar data (*13*). These hills, shown as VGG highs in red with an amplitude of ~80 Eötvös, are oriented west-east between fracture zones and transform faults, indicated by VGG lows in blue. By contrast, the Southeast Indian Ridge (SEIR) (Fig. 2B), with an intermediate spreading rate of 70 mm/year (*14*), features highly elongated abyssal hills filling the area between fracture zones, predominantly oriented northwest-southeast. The magnified circle highlights an individual abyssal hill in the blue box with length of ~300 km. A notable change in orientation near 66°W, 43°S, as in the black boxed area, reflects a change in spreading direction that can be used to improve plate reconstruction models. Fast-spreading ridges, such as the East Pacific Rise (EPR) (Fig. 2C), with a full spreading rate >130 mm/year (*15*), typically produce lower-amplitude (50- to 100-m root mean square height or 20 Eötvös), narrower-spaced, and more-elongated hills (*13*).

To validate the reliability of SWOT VGG data for mapping abyssal hill orientations, we compare the hand-picked orientations from multibeam sonar at 77 sites in the SEIR and 85 sites in the EPR with those derived from SWOT VGG (*10*). In both cases, the agreement is notable (figs. S1 and S2). For SEIR, the mean orientation

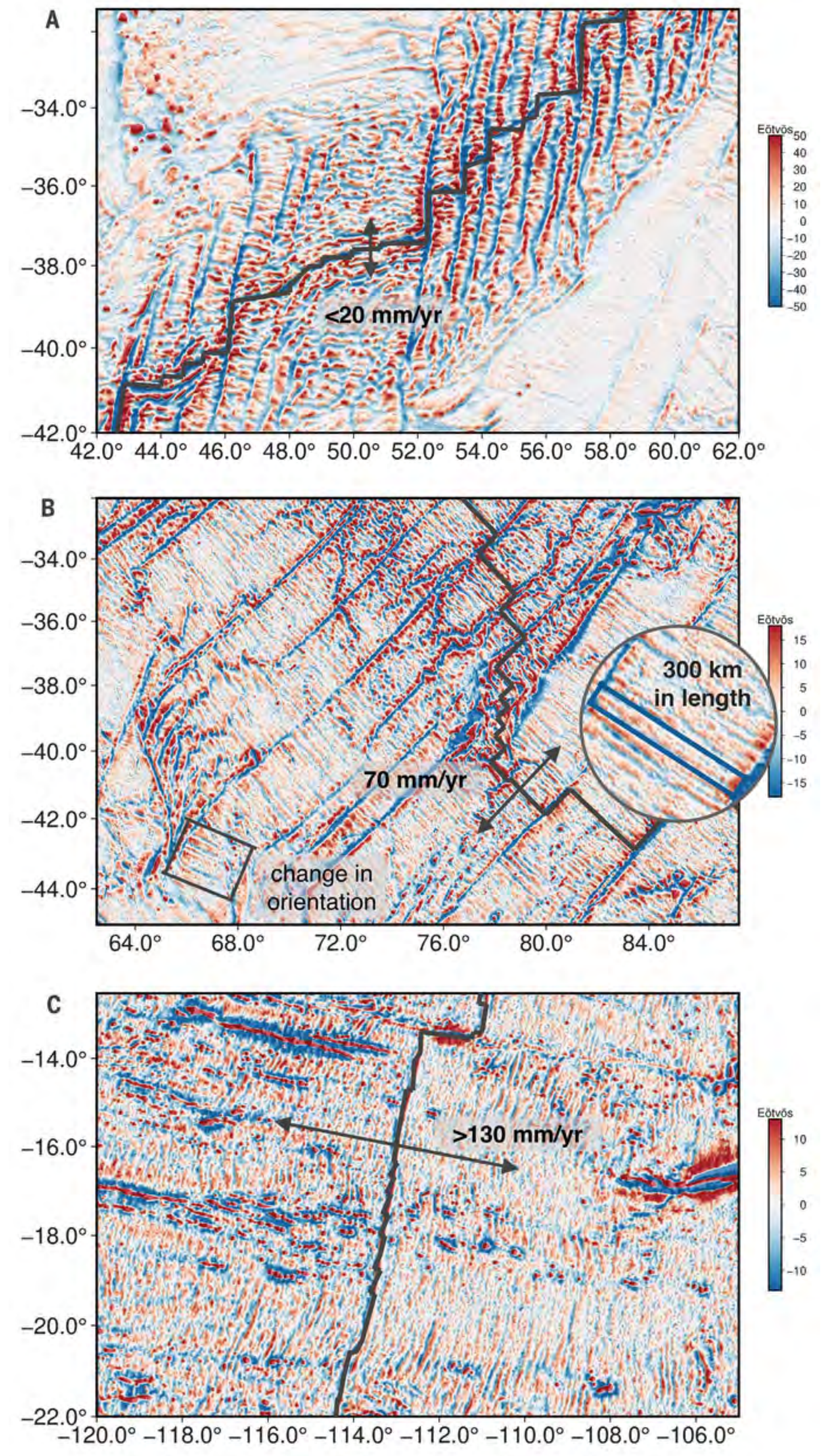

Fig. 2. Abyssal hills revealed by SWOT-derived global VGG. (**A** to **C**) Abyssal hills as elongated positive gravity anomalies are visible at the ultraslow spreading SWIR (A); the SEIR, where we highlight an unexpected long abyssal hill filling the space between two fracture zones (shown in the magnified circle) and a change in orientation (shown in the black box) (B); and the EPR (C). These maps highlight the orthogonal patterns of abyssal hills and fracture zones, with midocean ridges outlined in thick black, and plate separating direction indicated by black arrows.

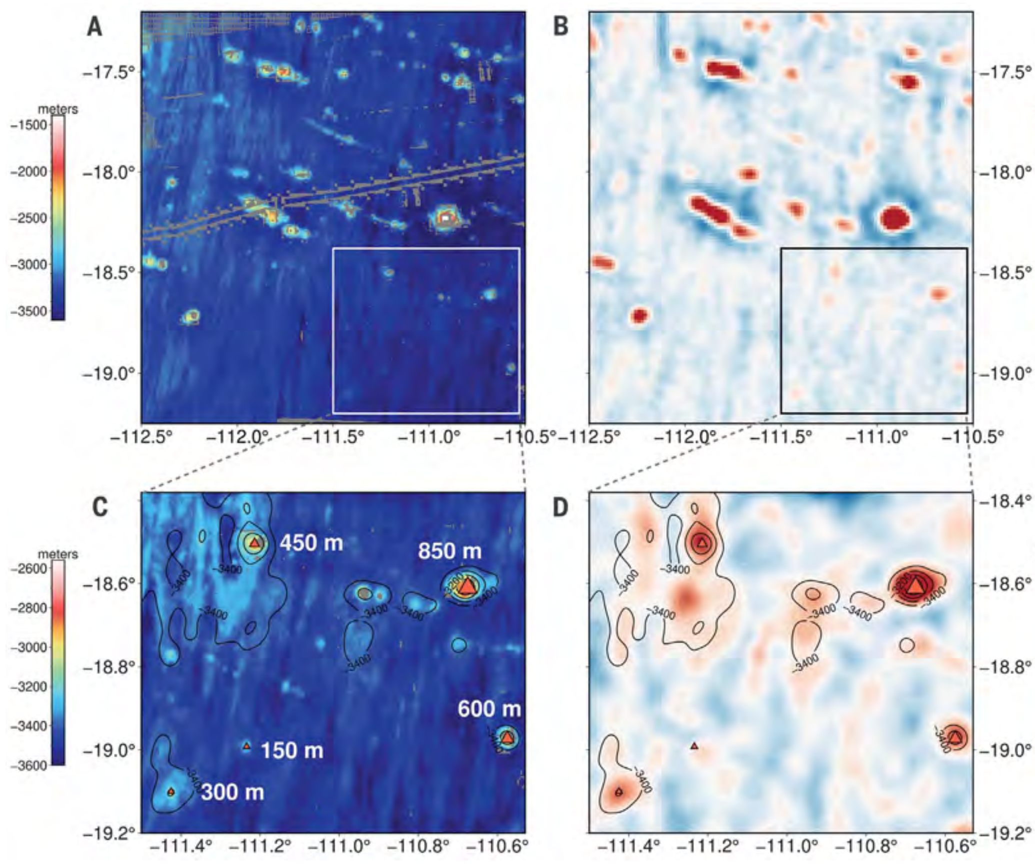

Fig. 3. Seafloor topography and VGG near the EPR, demonstrating that the smallest seamount resolvable by SWOT is about 450 m in height. (**A**) Seafloor topography from ship soundings (*31*) highlights seamounts with heights ranging between 500 and 2000 m (in red to white). Gray areas indicate uncharted regions. (**B**) These seamounts are readily identifiable as red peaks in the SWOT VGG map. (**C** and **D**) Seafloor topography (C) and SWOT VGG (D) of the boxed areas in (A) and (B), shaded with different color ranges and having contours of topography with 100-m intervals. Red triangles in (C) and (D) mark the centers of the five small seamounts, among which seamounts taller than 450 m are clearly identifiable by SWOT VGG. Seamounts smaller than 450 m in height have VGG values too small to distinguish from the orange peel background noise or abyssal hills.

difference is –0.89° with a standard deviation of 6.96°, and for the EPR, the mean orientation difference is 0.33° with a standard deviation of 6.55°. The largest discrepancy occurs in the southwest of the EPR, where the relatively narrow-swath multibeam coverage results in lower-accuracy orientation estimates. Orientation data for the SWIR are not provided owing to the short length of abyssal hills, which makes them difficult to depict accurately with multibeam data. These results confirm the reliability of SWOT in mapping abyssal hill orientations, thereby complementing traditional multibeam sonar measurements.

Small seamounts

Seamounts are undersea volcanoes that erupt from magmatic intrusions through the oceanic crust and are generated near midocean ridges, over upwelling plumes, and in ocean subduction zones (*16*). They influence ocean currents and nutrient distribution and often serve as biodiversity hotspots. Although the global distribution of large seamounts is well resolved by conventional nadir satellite altimetry, seamounts <1 km in height are mostly uncharted, relying on multibeam surveys for discovery.

With an 8-km spatial resolution, SWOT allows for the detection of small seamounts (<1 km in height) in regions lacking ship soundings. Figure 3A shows the seafloor topography surveyed by multibeam sonar, highlighting both large and small seamounts (using a red-to-white color gradient) above the surrounding abyssal ocean. For example, the largest seamount, ~2 km in height, is centered near longitude –110.9°, latitude –18.2° and is clearly observed by SWOT (Fig. 3B). It creates a circular-shaped positive VGG enclosed by a zero-crossing and the lithospheric flexure (negative VGG is shown as a blue ring), which is typical for an isostatically compensated seamount (*17*). To examine SWOT's limit in detecting small seamounts, we focus on a smaller area (Fig. 3, C and D) and mark the center of five seamounts with heights of 150 m, 300 m, 450 m, 600 m, and 850 m. Seamounts taller than 450 m are readily identified in SWOT VGG (Fig. 3D). The 150-m-tall seamount is indistinguishable from the so-called "orange peel" background noise. The 300-m-tall seamount, although creating positive VGG with the correct center, lacks the large gradient typically seen in seamounts, with a 0.25 height-to-radius ratio (*18*), and cannot be distinguished from abyssal hills (e.g., abyssal hill fabrics around longitude –111.25°, latitude –18.62°). SWOT, with its high-precision measurements from synthetic aperture radar (SAR) interferometry, enables the detection of even the smallest seamounts standing only 450 m tall, with a basal diameter of just 4 km (Fig. 3D) and at a typical ocean depth of 3500 m. The height-frequency distribution of seamounts is believed to follow a logarithmic distribution. One year of SWOT ocean measurement has the potential to substantially expand the global seamount catalog, increasing from the currently recorded 44,000 up to potentially 100,000 (*19*).

Continental margins

SWOT provides clear views at continental margins, especially in the high latitudes, revealing tectonic structures buried underneath sediments and ice. We show the comparison between VGG derived from 1 year of SWOT data and that from 30 years of nadir altimetry in Fig. 4. At the South America continental shelf adjacent to Argentina (Fig. 4, A and B), this region showcases the complex interplay between geological and sedimentary processes that shape passive continental margins. SWOT VGG (Fig. 4A) shows reduced noise and better-defined structures compared with traditional altimeter-derived VGG, which we refer to here as nadir VGG (Fig. 4B). West of the 500-m contour, the continental shelf consists predominantly of flat seafloor, where the VGG reveals basement structure that includes faults and sediment layers with widths of merely 6 km. The continental slope, situated between the 500-m and 1000-m contours, is an area characterized by sediment slumping and turbidity currents.

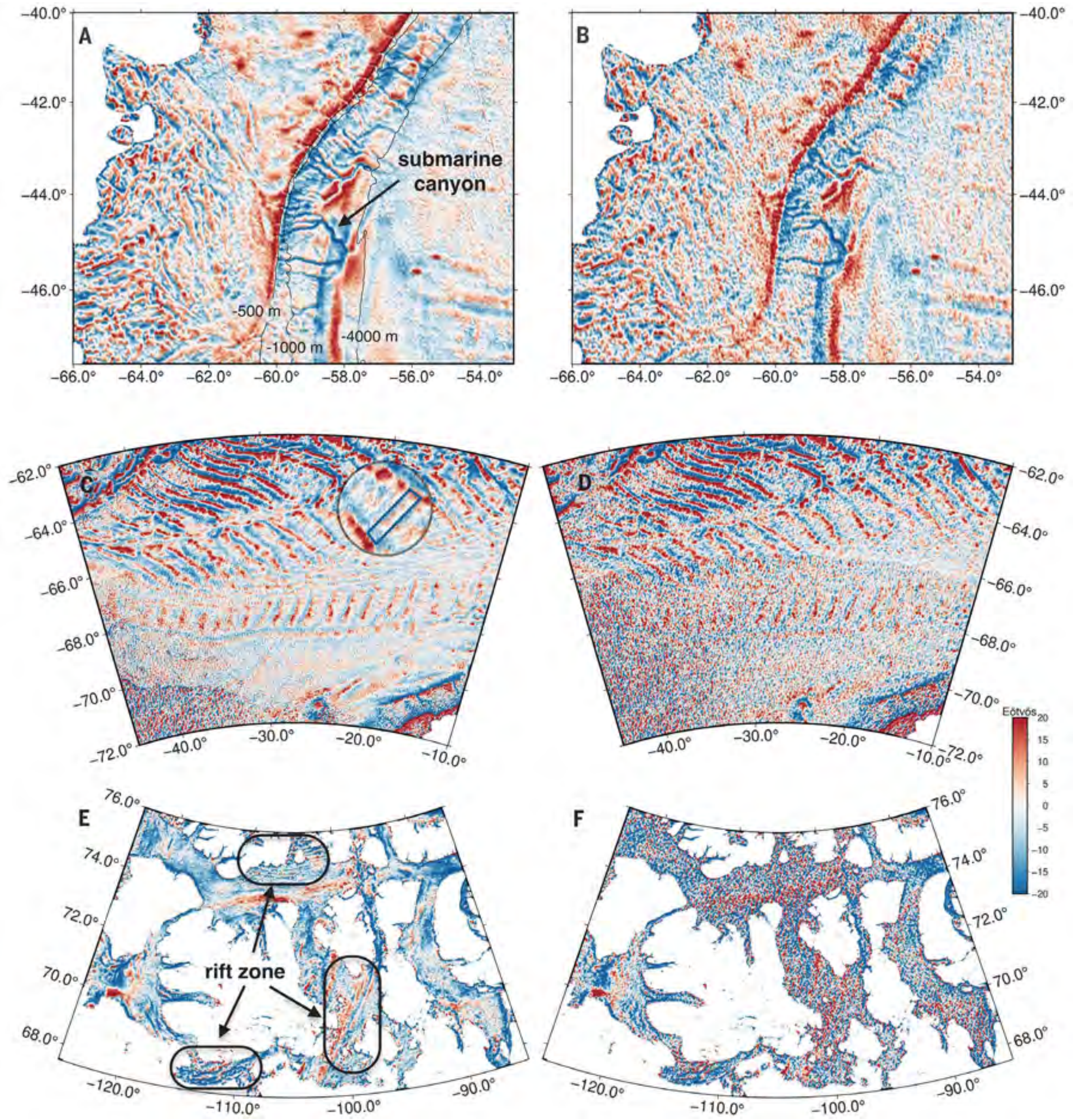

Fig. 4. Comparison between VGG derived from 1 year of SWOT data and that from 30 years of nadir altimetry at continental margins. Land area is in white. (**A** and **B**) Comparison in the South America continental shelf adjacent to Argentina. The 500-m, 1000-m, and 4000-m bathymetry contours are shown in faint black lines. Submarine canyons, which are ancient rivers, are clearly identifiable as VGG negatives with better-defined shapes. Edge effects from SWOT descending tracks orienting north-northwest to south-southeast can be seen in (A), which require further data editing. (**C** and **D**) Comparison at the Weddell Sea, where the herringbone structure along with the abyssal hills in between [e.g., VGG high in the blue polygon within the magnified circle in (C)], are clearly seen in SWOT. (**E** and **F**) Comparison at the Sverdrup Basin, located in the Canadian Arctic Archipelago, with rift zone structures labeled in black rounded boxes.

East of the 1000-m contour, the continental slope is carved by turbulent flows (visible as deep blue linear structures in the VGG map), carrying sediment to the deep Argentine basin (east of the 4000-m contour). These submarine canyons influence ocean currents and the distribution of nutrients in deep-sea environments.

The Weddell Sea (Fig. 4, C and D), located east of the Antarctic Peninsula, is a largely ice-covered region. The nadir VGG (Fig. 4D) resembles a mosaic image, especially south of 66°S owing to the lack of coverage from the Jason satellite series. By contrast, SWOT VGG (Fig. 4C) clearly shows the herringbone pattern, characterized by a series of fracture zones trending from northwest-southeast to north-northeast–south-southwest at about 67.5°S. The herringbone structure is closely linked to the three-plate spreading system involving South America, Africa, and Antarctica. This pattern represents a period of north-south spreading that later evolved into a more complex spreading regime, which led to the creation of new oceanic crust from the Late Jurassic to the Early Cretaceous (*20*). Abyssal hills in between the bones are beginning to appear, providing valuable insights for interpreting this region's tectonic development.

The Sverdrup Basin (Fig. 4, E and F), located in the Canadian Arctic Archipelago, is a major rift basin that developed in the Early Carboniferous period. Linear structures of alternating VGG highs and lows in black boxes are typical of rift zones, where extensional forces create faults, grabens, and horsts. SWOT VGG (Fig. 4E), having resolution of better than 8 km at continental margins, is not just superior to nadir VGG (Fig. 4F) but provides more details than airborne-surveyed gravity conducted at the circum-Arctic with 10 km–by–10 km grid resolution (*21*, *22*). Together with other geological and magnetic information, SWOT VGG can be used to refine the tectonic boundaries of the Arctic domain and provide useful information for future hydrocarbon exploration.

SWOT satellite: A sharper look on the seafloor

In a previous study (*23*), we evaluated the accuracy and resolution of the sea surface gradient derived from the 1-day repeat phase of

SWOT. The main conclusion of that paper was that the accuracy and resolution of the SWOT gradient exceed the accuracy and resolution of the best sea surface gradient models based on 30 years of nadir altimetry after just 10 repeat measurements. The ultimate accuracy of marine gravity from SWOT will be comparable to ship gravity measurement—~1.2 mgal, where 1 gal = 10^{-2} m/s^{-2}—and the spatial resolution will be around 8 km. These findings are consistent with both the current Version C and the upcoming Version D of the SWOT ocean data because no fundamental changes have been made to the KaRIn phase measurements across versions. The along-track slope is slightly more accurate than the cross-track slope, and the accuracy of gradients from individual cycles degrades with increasing significant wave height. Additionally, the accuracy of the slope measurements is best in the center of each of the two swaths and worst near the edges of the swaths. A total of 18 cycles were available for averaging, which explains why the SWOT VGG map is better than the best map based on 30 years of nadir altimetry. The spatial distribution of repeated measurements is not uniform, with many repeats at high latitudes, where the satellite tracks converge, and ~18 repeats near the equator. Because SWOT cannot make measurements within ~8 km on either side of nadir, there are diamond-shaped gaps (fig. S3) in coverage that will never be filled unless the 21-day orbit is changed (*10*).

These improvements in accuracy and resolution of the SWOT gravity field will have major implications for the prediction of seafloor depth in regions devoid of ship soundings. One key step in the depth prediction algorithm is the downward continuation of the high-pass filtered gravity to the regional ocean floor depth (*24*). A length scale parameter controls the low-pass filter wavelength versus mean ocean depth. Using SWOT VGG, this parameter can be reduced to enable prediction of much smaller scale structures—perhaps by a factor of 2 in each dimension. Of course, the VGG in the diamond-shaped gaps will have lower resolution and could result in a prediction with diamond-shaped artifacts. Future processing of SWOT data should strive to minimize the size of these gaps through more-careful editing of the 250-m-resolution ocean product.

One major advancement in marine gravity with SWOT is its clear view of abyssal hills, which enables the global characterization of these features. As discussed above, the abyssal hills are created at midocean ridges by ridge-parallel normal faulting and volcanism. Because these elongated hills are rafted across the ocean basins by plate motions, they retain information about the paleo spreading direction. Abyssal hill signatures are ubiquitous in the deep oceans, except when they are overprinted by volcanism or intraplate deformation. They can even be observed in regions with thick sediment covers. A global analysis of the orientations of the abyssal hills will provide an important type of data for refining plate reconstruction models (*25*).

The interaction of deep ocean tides with abyssal hills, especially along rough, slow-spreading ridges, generates high-mode internal tides that are prone to shear instability and local breaking. Small but abundant, these ubiquitous features contribute substantially to deep ocean mixing, accounting for 12% globally (*26*, *27*). We performed a simulation study, using synthetic high-resolution topography (*28*) and a semianalytical method (*29*). The preliminary results show that deep ocean mixing from high-mode internal tide local breaking is highly sensitive to the orientation of topographic features (fig. S4). A 20° error in abyssal hill orientation can lead to a >15% variation in both individual modes and total conversion rates (*10*). A global abyssal hill orientation map derived from the SWOT VGG will refine the estimates of deep ocean mixing.

Conclusions

Measurements of SSH from traditional satellite altimetry have provided low-resolution (12- to 16-km wavelength) mapping of the gravity field over the 75% of the seafloor not surveyed by ships. The altimetry data provided by SWOT have improved the spatial resolution of the marine gravity by a factor of ~1.5, except at the highest northern latitude (>77.6°, not covered by SWOT) and in small diamond shaped gaps in coverage from the 21-day science orbit. The spatial resolution of the marine gravity will continue to improve for as long as the satellite operates. The ultimate resolution is controlled by the natural upward continuation of gravity field from the seafloor, so it will depend on the regional ocean depth; shallow continental margins could have a spatial resolution of 4 km, whereas the resolution will be 7- to 9-km wavelength in the deep ocean. The implications of SWOT VGG mapping are profound: The resolved abyssal hills will be used to revise the global plate reconstruction models, the number of mapped seamounts may double, and global bathymetry maps will have a factor of 2 improvement in resolution in the 75% of the seafloor not mapped by ships. The improved bathymetry will be used to refine numerical models of deep ocean currents and the generation of high-mode, tidally generated internal waves, which are important for deep ocean mixing and the uptake of heat and CO_2 in the ocean.

REFERENCES AND NOTES

1. L. Mayer *et al.*, *Geosciences* **8**, 63 (2018).
2. W. H. Smith, D. T. Sandwell, *Science* **277**, 1956–1962 (1997).
3. K. Picard, B. Brooke, M. F. Coffin, *Eos* **98**, EO069015 (2017).
4. D. T. Sandwell, H. Harper, B. Tozer, W. H. F. Smith, *Adv. Space Res.* **68**, 1059–1072 (2021).
5. L.-L. Fu *et al.*, *Geophys. Res. Lett.* **51**, e2023GL107652 (2024).
6. D. T. Sandwell, R. D. Müller, W. H. Smith, E. Garcia, R. Francis, *Science* **346**, 65–67 (2014).
7. D. L. Turcotte, G. Schubert, *Geodynamics* (Cambridge Univ. Press, 2002).
8. Surface Water Ocean Topography (SWOT), SWOT Level 2 KaRIn Low Rate Sea Surface Height Data Product, version 2.0, PO.DAAC (2024); https://doi.org/10.5067/SWOT-SSH-2.0.
9. "SWOT Science Data Products: User Handbook" (Jet Propulsion Laboratory, JPL D-109532, 2024); https://www.earthdata.nasa.gov/s3fs-public/2024-06/D-109532_SWOT_UserHandbook_20240502.pdf.
10. Materials and methods are available as supplementary materials online.
11. H. W. Menard, J. Mammerickx, *Earth Planet. Sci. Lett.* **2**, 465–472 (1967).
12. W. R. Buck, A. N. Poliakov, *Nature* **392**, 272–275 (1998).
13. J. A. Goff, *Geophys. Res. Lett.* **47**, e2020GL088162 (2020).
14. R. D. Müller, M. Sdrolias, C. Gaina, W. R. Roest, *Geochem. Geophys. Geosyst.* **9**, Q04006 (2008).
15. D. B. Rowley *et al.*, *Sci. Adv.* **2**, e1601107 (2016).
16. P. Wessel, in *Seamounts: Ecology, Fisheries & Conservation*, T. J. Pitcher *et al.*, Eds. (Blackwell Publishing, 2007), pp. 1–25.
17. P. Wessel, *Science* **277**, 802–805 (1997).
18. J. Gevorgian, D. T. Sandwell, Y. Yu, S. S. Kim, P. Wessel, *Earth Space Sci.* **10**, e2022EA002331 (2023).
19. P. Wessel, D. T. Sandwell, S. S. Kim, *Oceanography* **23**, 24–33 (2010).
20. L. C. Kovacs, P. Morris, J. Brozena, A. Tikku, *Tectonophysics* **347**, 43–64 (2002).
21. C. Gaina, S. C. Werner, R. Saltus, S. Maus, CAMP-GM Group, in *Arctic Petroleum Geology*, A. M. Spencer, A. F. Embry, D. L. Gautier, A. V. Stoupakova, K. Sørensen, Eds. (Geological Society of London, 2011), pp. 39–48.
22. S. Kenyon, R. Forsberg, B. Coakley, *Eos* **89**, 289–290 (2008).
23. Y. Yu, D. T. Sandwell, G. Dibarboure, C. Chen, J. Wang, *Earth Space Sci.* **11**, e2024EA003581 (2024).
24. W. H. F. Smith, D. T. Sandwell, *J. Geophys. Res.* **99**, 21803–21824 (1994).
25. K. J. Matthews, M. Seton, R. D. Müller, *Earth Planet. Sci. Lett.* **355-356**, 283–298 (2012).
26. A. Melet, S. Legg, R. Hallberg, *J. Clim.* **29**, 3473–3500 (2016).
27. C. Vic *et al.*, *Nat. Commun.* **10**, 2099 (2019).
28. D. T. Sandwell *et al.*, *Earth Space Sci.* **9**, e2021EA002069 (2022).
29. S. G. Llewellyn Smith, W. R. Young, *J. Phys. Oceanogr.* **32**, 1554–1566 (2002).
30. Y. Yu, Datasets for Abyssal Marine Tectonics from the SWOT Mission, Zenodo (2024); https://doi.org/10.5281/zenodo.13315574.
31. GEBCO Bathymetric Compilation Group, The GEBCO_2024 Grid - A continuous terrain model of the global oceans and land, NERC EDS British Oceanographic Data Centre NOC (2024); https://doi.org/10.5285/1c44ce99-0a0d-5f4f-e063-7086abc0ea0f.
32. Y. Yu, Source Codes for Abyssal Marine Tectonics from the SWOT Mission, Zenodo (2024); https://doi.org/10.5281/zenodo.13315565.

ACKNOWLEDGMENTS

We appreciate the internal review by H. A. Fricker and communication with C. Chen. The SWOT mission is jointly developed by NASA and CNES with contributions from the Canadian Space Agency (CSA) and the United Kingdom Space Agency. **Funding:** This research was supported by the following programs: the Eric and Wendy Schmidt AI in Science Postdoctoral Fellowship (a program of Schmidt Sciences), the NASA SWOT program grants NNX16AH64G and NNX16AH67G, the Office of Naval Research, and the University of New Hampshire subaward no. PZL0355 (Prime: Sasakawa Peace Foundation). **Author contributions:** Conceptualization: Y.Y. and D.T.S. Methodology: Y.Y., D.T.S., and G.D. Investigation: Y.Y. and D.T.S. Visualization: Y.Y. and D.T.S. Funding acquisition: D.T.S. Supervision: D.T.S. Writing – original draft: Y.Y. and D.T.S. Writing – review & editing: Y.Y., D.T.S., and G.D. **Competing interests:** The authors declare no competing interests. **Data and materials availability:** The SWOT L2 ocean data Version C was downloaded from Earthdata on 25 July 2024 (*7*). The dataset and codes generated for data processing and plotting in the paper are available at Zenodo (*30*, *32*).

SUPPLEMENTARY MATERIALS

science.org/doi/10.1126/science.ads4472
Materials and Methods
Figs. S1 to S5

Submitted 14 August 2024; accepted 22 October 2024
10.1126/science.ads4472